

# Simultaneous Primer Coating for Fast Drying of Battery Electrodes

David Burger,\* Noah Keim, Junaid Shabbir, Yuhao Gao, Marcus Müller, Werner Bauer, Alexander Hoffmann, Philip Scharfer, and Wilhelm Schabel

Primers are used to promote adhesion and reduce electrical interface resistance. Normally, the process of applying primer and electrode coating happens in two separate, sequential steps. Herein, primer and electrode are applied simultaneously, wet-in-wet. For fast drying of electrode coatings, a binder-redistribution by binder migration happens. A normally unwanted binder migration is tried to be utilized. The goal is to use less binder in the electrode coating and dry it faster without losses in adhesion and performance. By using simultaneous primer coatings incorporating LAPONITE, the adhesion can be promoted by over 200%. This allows to eliminate the styrene-butadiene-rubber-binder in the electrode slurry, saving in total of 70% of the binder. For eight times faster drying up to 30% improved specific capacity at 2C can be shown. This promising approach shows potential for any materials that lack adhesion, extending it, e.g., to porous, nanostructured particles and materials used in sodium-ion batteries.

the migration of binder. Addressing this issue in the context of material efficient processing, we want to facilitate a primer layer between the substrate and the active layer, not to suppress binder migration itself, but to limit the use of binder only to the substrate- electrode interface. Sequentially coated multilayer electrodes with a primer as bottom layer have been shown to exhibit better adhesion, electrical conductivity, and discharge capacity compared to single-layer electrodes manufactured at the same drying rate.<sup>[2,3]</sup> However, as state-of-the-art an additional coating and drying step is needed for applying the primer. To overcome this, we investigate simultaneously coated multilayers (coating of both layers in the same process) with a primer as a functional bottom layer.

With this research, we aim to provide insights into the drying of simultaneously coated multilayers for varying formulations, their mechanical properties and electrochemical performance, facilitating a design of multilayers applicable for large-scale electrode production.

## 1. Introduction

The lithium-ion battery (LIB) has emerged as a crucial energy storage system in electric vehicles. The global demand for LIBs in electric vehicles is projected to vastly increase, reaching 4700 GWh by 2030.<sup>[1]</sup> To meet this rising demand, the production of LIBs must expand while reducing costs.


In this study, we explore a potential cost-reduction strategy by increasing the drying rate during electrode production from a process-structure-property perspective. Almost generally, elevated drying rates compromise electrode adhesion, leading to coating delamination and reduced C-rate capability due to

### 1.1. Primer Coatings

A primer coating,<sup>[2–6]</sup> usually applied in a separate process before the actual coating, is a functional layer between the main coating (here electrode coating) and the current collector. It offers improved contact between the electrode coating and the current collector. Both mechanical (increased adhesion strength) and electrical (reduced interface resistance) properties should be improved by a primer. For a battery electrode, a primer coating can help to enhance the overall stability of the active material on the current collector, leading to improved durability and enhanced long-term performance.<sup>[2]</sup> Comprising binders, e.g., the sodium salt of carboxymethyl cellulose (CMC) and styrene-butadiene-rubber (SBR), the primary purpose of a primer is to significantly increase the adhesion between the coating and the current collector. Conductive additives like carbon black (CB) or carbon nanotubes can be added to the primer<sup>[4–6]</sup> to decrease the surface resistance especially for cathode materials with low electric conductivity. Given an adequate (low) amount of binder on the current collector, also approaches of foil pretreatment with solely binder exist.<sup>[3]</sup> Although the functional layer does not contribute to capacity (has no active material), its thin thickness (0.1–10 μm)<sup>[5]</sup> minimally influences the overall electrode volumetric and gravimetric energy density (1–2 g m<sup>-2</sup> areal mass loading).<sup>[5]</sup>

D. Burger, J. Shabbir, Y. Gao, A. Hoffmann, P. Scharfer, W. Schabel  
Thin Film Technology (TFT)  
Karlsruhe Institute of Technology (KIT)  
Straße am Forum 7, D-76131 Karlsruhe, Germany  
E-mail: david.burger@kit.edu

N. Keim, M. Müller, W. Bauer  
Institute for Applied Materials (IAM)  
Karlsruhe Institute of Technology (KIT)  
Hermann-von-Helmholtz-Platz 1, D-76144 Eggenstein-Leopoldshafen,  
Germany

 The ORCID identification number(s) for the author(s) of this article can be found under <https://doi.org/10.1002/ente.202401668>.

© 2024 The Author(s). Energy Technology published by Wiley-VCH GmbH. This is an open access article under the terms of the Creative Commons Attribution License, which permits use, distribution and reproduction in any medium, provided the original work is properly cited.

DOI: 10.1002/ente.202401668

To be industrially relevant for electrode production, the processing speed for a production line of primer-coated current collector must be high in coating as well as in drying. Possible application methods are gravure,<sup>[4]</sup> roll,<sup>[5]</sup> or slot-die<sup>[2,7]</sup> coating in high-speed application.

Inspired by commercial availability of primed foils, most of the literature deals with sequential processing,<sup>[2,8]</sup> that means production of a primed substrate and processing of electrodes on it.

In this study, we focus on identifying the properties required for primer slurries to enable processing in a simultaneously coated multilayer approach. The aim is to facilitate beneficial electrode properties, particularly under conditions of high drying rates.

By comparison of three formulations “Primer A–C”, we analyze the impact of the primer composition on the processing and microstructure formation during drying. To do so, we use the full picture of cryo-scanning electron microscopy (cryoSEM) and optical imaging of the microstructure formation as well as indirect measurement methods like adhesion strength- and resistivity measurement, C-rate capability, and long-term cycling tests.

### 1.2. Challenges in Drying

The biggest challenge for fast drying of battery electrodes is the migration of binder by capillary action during drying. An accumulation of binder material at the top of the electrode is known to increase the ionic resistance and limit C-rate capability. In literature, multilayer structures are presented to mitigate the migration.<sup>[9,10]</sup> Most simultaneously coated multilayer architectures in literature have similar properties regarding solid content, the same order of magnitude in viscosity or only little grading in terms of binder concentrations.<sup>[9,11–14]</sup> The drying of these structures can be significantly influenced, e.g., by the choice of different particle’s size and morphology that influence mostly the pore emptying during the capillary stage of drying.<sup>[9,10]</sup> Kumberg et al.<sup>[10]</sup> have presented simultaneously coated multilayer anodes with smaller, spherical graphite in the bottom layer (less binder migration, retention of solvent from capillary transport) and a top layer composed of bigger spherical graphite (better for formation of the solid electrolyte interphase). It can be assumed that the drying of multilayers with a primer as bottom layer (only CB, binders, and water) shows a very different drying behavior. The main differences to multilayers comprising two battery slurries are firstly the lower solid content in the primer (here 8-times) and secondly the lack of a capillary porous network of the same scale as in the electrode top layer (nm-scale for primer vs  $\mu\text{m}$ -scale for active material). Furthermore, multilayers with solvent gradients have been reported to be challenging in terms of microstructure homogeneity after drying.<sup>[13]</sup> We assume a significant amount of migration of primer into the porous structure of the graphite layer. Having to accept this, microstructure optimization must find a new approach not to mitigate, but to work around binder migration.

### 1.3. Formulation and Microstructure Optimization

Key promising advantage of a primer is the improved contact between the electrode coating and the substrate, intended for both mechanical (adhesion strength) and electrical connection (interface resistance). To achieve a high adhesion strength, the

additive LAPONITE is known to improve the adhesion of battery electrode coatings.<sup>[15,16]</sup> Preliminarily used as rheological modifier, its interaction with CMC leads to a highly shear-thinning behavior and a network formation with gel-like behavior. Its use to enhance the adhesion strength of battery electrodes may be ambivalent. We have reported increases in ionic resistance for graphite anodes in a previous publication.<sup>[15]</sup> However, contained in a functional layer near the substrate it is promising for the formation of a network that can partially withstand capillary action during drying. As shown by Hofmann et al. (2024), the SBR mass fraction has crucial impact on the electrochemical performance of CMC/SBR-based graphite anodes.<sup>[17]</sup> Combined with reducing the binder content of the battery electrode coating we expect improvements in electrochemical performance for electrodes with simultaneously coated primer, if there is generally less binder that can migrate. With the simultaneously coated primer it may be possible to fully forego SBR usage in the electrode coating and just use a small amount in the primer. **Table 1** shows the composition of electrode slurries with decreasing fractions of SBR within the graphite layer we tested.

## 2. Results and Discussion

### 2.1. Primer Formulation

Three different primer formulations “A–C” are investigated in this study (**Table 2**). The formulation “Primer A” is based on a primer formulation in literature, which has been shown to be applicable for slot-die coating.<sup>[2]</sup> A subsequent increase in viscosity is reached by an increase in solid content with “Primer B” and the use of the rheology additive LAPONITE with “Primer C”.

The different primers were all characterized by shear-rheometry. **Figure 1** shows the shear behavior for the slurry “SBR100” and the primer slurries “Primer A–C” for a backward hysteresis outgoing from preshearing with a shear rate of  $1000\text{ s}^{-1}$ .

The primers differ in their flow behavior. The change in formulation from “Primer A” to “Primer B” leads to an increase in

**Table 1.** Composition of the electrode slurries used. SBR100 is the starting point for a stepwise reduction of SBR content.

	Active				Solids wt-%	Density (solids) $\text{kg m}^{-3}$
	Graphite [wt-%]	CB [wt-%]	CMC [wt-%]	SBR [wt-%]		
SBR100	93.00	1.40	1.87	3.73	43.00	2153
SBR50	94.86	1.40	1.87	1.87	43.00	2194
SBR0	96.73	1.40	1.87	–	43.00	2236

**Table 2.** Composition of aqueous primers.

	Graphite	CB	CMC	SBR	LAPONITE-RD	Solids wt-%	Density $\text{kg m}^{-3}$
	wt-%	wt-%	wt-%	wt-%	wt-%		
Primer “A”	–	33.30	33.30	33.30	–	2.5	1453
Primer “B”	–	20.00	26.70	53.30	–	5.0	1320
Primer “C”	–	18.80	25.00	50.00	6.30	5.4	1360

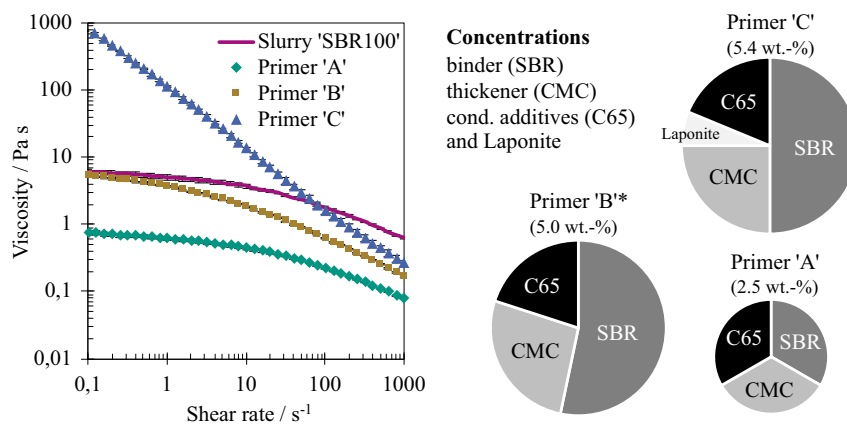


**Figure 1.** Viscosity versus shear rate for the slurry “SBR100” and the primers “Primer A–C” for a backward hysteresis outgoing from a preshearing with a shear-rate of  $1000\text{ s}^{-1}$ . “Primer C” shows toward low shear rates a high apparent viscosity due to network formation by LAPONITE. Pie charts resemble the concentrations and proportions of CB, CMC, SBR, and LAPONITE in the primers. \*Primer B is oriented on the composition of slurry SBR100, minus graphite. The proportions and concentrations of CB, CMC, and SBR are equal (8:4:3, Table 1).

viscosity over the complete shear–rate range, mostly driven by the higher solid content. Comparing “Primer B” and “SBR100”, the proportions and concentrations of CB, CMC, and SBR are equal (8:4:3, Table 1). The viscosity reaches almost the same value for low shear rates. In this shear-rate range, the viscosity is dominated by the network of thickener CMC and CB. A further increase in low-shear viscosity is obtained using LAPONITE in “Primer C”. It shows a very strong shear-thinning behavior with an apparent viscosity at low shear rates after the yield point is undercut. The strong network formation fits to previous investigations using the additive in a graphite anode slurry.<sup>[15]</sup> From literature it is known that for simultaneous slot-die coating the viscosity ratio between the slurries determines coating stability.<sup>[18]</sup> The influence of Laponite on the shear thinning of primer slurries could open new possibilities for investigations in this field.

## 2.2. Simultaneously Coated Primer Layer

With primer formulations of varying flow behavior and formulation, the question arises, which of them is the most suitable to achieve improved contact to the substrate foil. Electrodes were produced using “Primer A–C” together with the anode slurry “SBR100” as top layer by simultaneous multilayer coating and the best primer was identified (Section 2.2). The drying of the selected primer is further characterized (Section 2.3), and it is combined with “SBR50” and “SBR0” for optimization of the electrochemical properties of the electrodes (Section 2.4). All primers and electrode coatings were coated by knife coating on a copper substrate and formed homogeneous films. For simultaneous multilayer coating in the laboratory scale, the wet film is subsequently passed from one knife coating station to another. The areal mass loading of the primer (predetermined by just coating a primer layer) was about  $1\text{--}2\text{ g m}^{-2}$  with a film thickness of  $\approx 1\text{--}3\text{ }\mu\text{m}$  (only primer, dry). Data for the porosity of the primers and the multilayer electrodes are summarized in Table 3.

To achieve structural optimization of the electrode that is industrially relevant, it is essential to characterize the impact of the coating and its behavior for faster drying at higher drying

rates. Quantitative measures, such as adhesion and resistivity measurements, can provide a foundation for optimization. The adhesion strength of single-layer electrodes serves as a reference of binder distribution and changes in the electrode’s microstructure for increasing drying rate.<sup>[19–22]</sup> Figure 2 shows the adhesion strength of the simultaneously coated multilayer electrodes “SBR100 on Primer A–C” made with the slurry “SBR100” as top layer and varying primer “Primer A–C” as bottom layer for increasing drying rate. The “Single Layer SBR100” electrodes act as a reference.

For all multilayers, a decrease in adhesion strength with increasing drying rate is observed. Binder migration is present not only for the “Single Layer SBR100”, but also for the multilayers that contain the respective primer as bottom layer. The multilayers show very different absolute values for the adhesion strength. “SBR100 on Primer A” leads, in contrast to the expectation from a sequential processing in literature,<sup>[2,3]</sup> in simultaneous processing to a lower adhesion strength than “Single Layer SBR100”. For “SBR100 on Primer B” a 55% adhesion-strength

**Table 3.** Primer and electrode characterization regarding dry film thickness, areal mass loading, and porosity. Given is the average and standard deviation over all drying settings and samples. This includes single-layer coatings and simultaneous multilayer coatings.

	Thickness	Porosity <sup>a)</sup>	Multilayer electrodes		
			Top layer: SBR100, SBR50 or SBR0		
			Bottom layer: Primer A, B or C		
	(only primer, dry)	(only primer, dry)	Loading	Thickness	Porosity <sup>b)</sup>
Primer A	$2 \pm 1\text{ }\mu\text{m}$	$\approx 30\text{--}40\%$	$121 \pm 3\text{ g m}^{-2}$	$139 \pm 2\text{ }\mu\text{m}$	$60 \pm 3\%$
Primer B	$2 \pm 1\text{ }\mu\text{m}$	$\approx 50\text{--}70\%$			
Primer C	$2 \pm 1\text{ }\mu\text{m}$	$\approx 15\text{--}30\%$			

<sup>a)</sup>Values vary highly because of the low dry film thickness. Hence, just an interval is given. <sup>b)</sup>Porosity error is calculated by error propagation with  $\pm 2\text{ }\mu\text{m}$ ,  $\pm 4\text{ g m}^{-2}$ , and  $\pm 25\text{ g m}^{-3}$ .

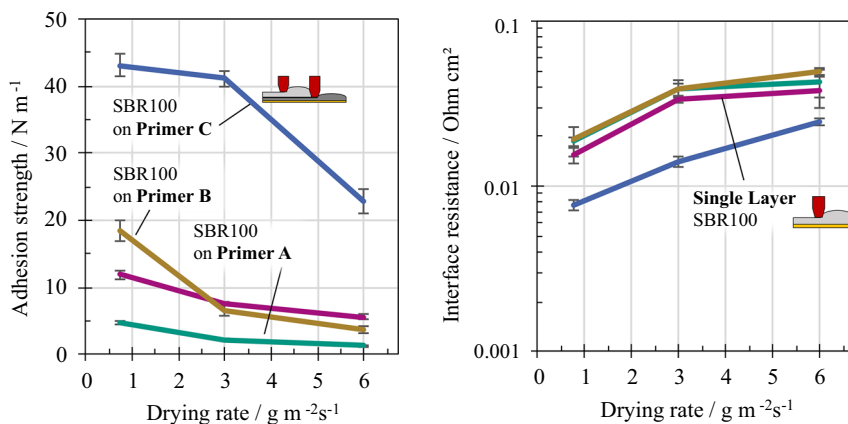


**Figure 2.** Adhesion strength and electrical interface resistance versus drying rate for simultaneously coated multilayers “SBR100 Primer A–C” made with the slurry “SBR100” as top layer and varying primer “Primer A–C” as bottom layer. Comparison to “Single Layer SBR100” electrodes. “SBR100 on Primer C” yields a several times higher adhesion strength although binder migration is indicated for all systems by a loss of adhesion strength with increasing drying rate. Only the multilayer “SBR100 on Primer C” can provide a significantly lower interface resistance than the “Single Layer SBR100”.

increase is gained compared to “Single Layer SBR100” at  $0.75 \text{ g m}^{-2}\text{s}^{-1}$  which is followed by an alignment toward higher drying rates. Similar values were expected as the composition of the “Primer B” is equal to the passive material composition of the slurry “SBR100” used for the single layer. In contrast, the use of “Primer C” in the simultaneously coated multilayer leads to a significant adhesion increase of around 260% at  $0.75 \text{ g m}^{-2}\text{s}^{-1}$  and even more at increasing drying rate. Delamination was observed to happen even inside graphite particles (S2, Supporting Information). A higher proportion of primer and therefore binder is thought to remain at the interphase between current collector and electrode coating suggested by the remain on the peeled-off foil (S1, Supporting Information). The remain of primer has also beneficial effects on the interface resistance, which is significantly reduced compared to the “Single Layer SBR100”. This behavior is special for “Primer C” as for comparing the interface resistance of “SBR100 on Primer A” and “SBR100 on Primer B” with “Single Layer SBR100” no significant benefits are gained.

To see if there is a closed, stable layer of primer on the copper substrate for increasing the drying rate, **Figure 3** shows a SEM micrograph of the simultaneously coated multilayer “SBR100 on Primer C” for drying rates of  $0.75 \text{ g m}^{-2}\text{s}^{-1}$  (lower drying rate, LDR) and  $6 \text{ g m}^{-2}\text{s}^{-1}$  (higher drying rate, HDR).

The SEM images (bottom) show that the multilayer coating was carried out successfully with a high proportion of CB and binder between the graphite active material and the copper substrate. A comparison of the bottom regions for increasing drying rate suggests a thicker primer layer (more contact points to graphite) in case of the lower drying rate, which is in accordance with the trend of adhesion strength with increasing drying rate. In case of the higher drying rate, the primer layer is less closed and generally smaller. However, still, enough binder remains to significantly elevate the adhesion strength compared to the single layer. By the binder migration from out of the electrode coating as well as from out of the primer layer, binder accumulates at the top of the electrode for faster drying at higher drying rate.

### 2.3. Drying Mechanism for Simultaneously Coated Primer Coatings

In the drying investigation, we want to visualize, how the film shrinkage and pore emptying behavior of multilayers with very different solvent content and order of magnitude for particle sizes behave. It is conceivable that capillary-driven solvent transport will impact the microstructure formation of multilayer electrodes made with varying primer differently. The intention of a detailed comparison of the drying behavior of “SBR100 on Primer A” and “SBR100 on Primer C” with “Single Layer SBR100” (most different) is to gain indications which properties of the primer slurry influence the migration behavior.

For a simultaneous primer coating (no active material in the bottom layer), the pore emptying behavior known for single layers in literature<sup>[23]</sup> (same composition as “SBR100”), might be altered. To observe the pore emptying, a digital microscope was used to acquire images through a transparent substrate.<sup>[23]</sup> **Figure 4** shows a horizontal cross-sectional view on the bottom of the coatings through a glass substrate for times close to the beginning of the pore emptying and close to the end of the pore emptying.

“Single Layer SBR100” shows the pore-emptying behavior that is described in literature for this formulation.<sup>[23]</sup> “SBR100 on Primer A” and “SBR100 on Primer C” show a pore emptying in the same order of magnitude regarding pore sizes, despite no graphite is in direct contact with the glass plate directly after coating (darker gray of primer than for graphite slurry). However, the timing and the structure of the porous network differ. This can be observed by comparing images at the beginning of the pore emptying. “SBR100 on Primer A” and “Single Layer SBR100” show already very pronounced emptying in clusters, while “SBR100 on Primer C” shows only partial and very limited pore breakthroughs to the substrate. The fact that capillary transport (driving mechanism for pore emptying) can be observed by appearance of empty pores at the substrate shows that the wet primer coating must be partially penetrated by graphite. Otherwise, no capillary transport of primer into the electrode coating would be possible, because it relies on solvent menisci to act. The



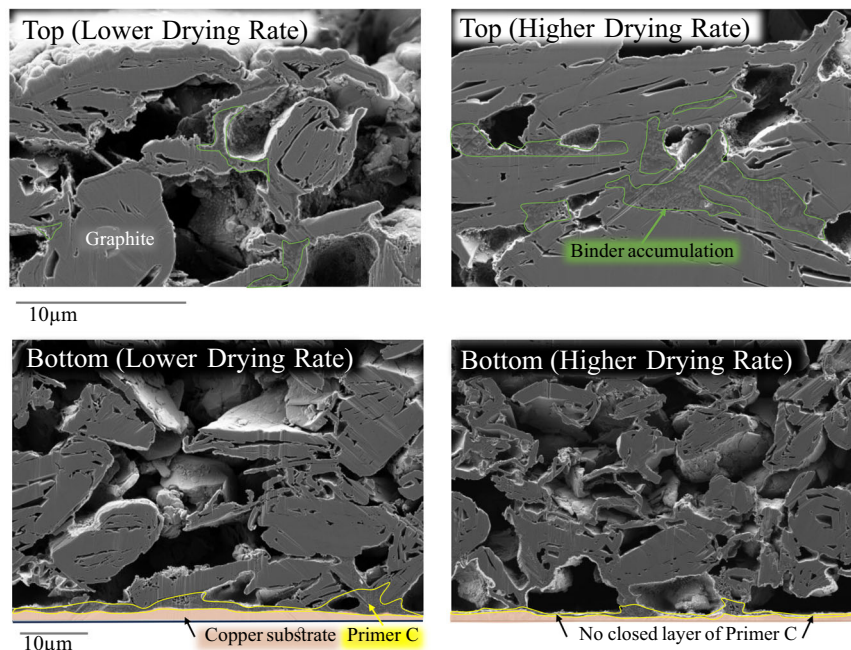


**Figure 3.** SEM micrograph of a cross-section of the multilayer “SBR100 on Primer C” dried with  $0.75 \text{ g m}^{-2}\text{s}^{-1}$  (LDR) and  $6 \text{ g m}^{-2}\text{s}^{-1}$  (HDR). The primer coating on the copper foil only forms an almost closed layer at LDR. There is an accumulation of binder, noticeable at the top of the electrode dried at HDR.

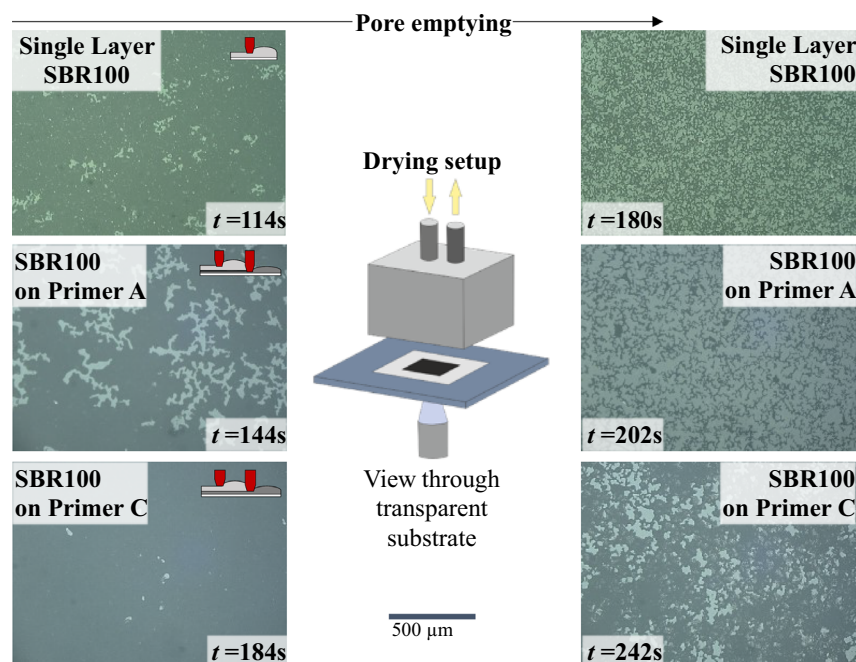


**Figure 4.** Pore emptying behavior of “Single Layer SBR100”, as well as the multilayers “SBR100 on Primer A” and “SBR100 on Primer C” dried with  $0.75 \text{ g m}^{-2}\text{s}^{-1}$ . The times are chosen at 10% and 90% between the observation of the first empty pore (106, 138, 178 s) and no further change observable (190, 210, 250 s) in the pore emptying video. They do not necessarily match with the end of the drying process. Pictures are shown in color at the same light-exposure settings.

contact area between coating and glass substrate seems to be greater in the case of “SBR100 on Primer C” than in the case of “Single Layer SBR100”. This falls in line with the much greater adhesion strength for “SBR100 on Primer C”. Compared to

“Primer A” and “Primer B”, we believe that the accountable property of “Primer C” for having a higher residue near the substrate is the network formation between LAPONITE and CMC. It gives the primer resistance against removal by capillary transport.

The question arises if the capillary transport is limited just due to the primers flow behavior or is additionally due to a later pore breakthrough. A delayed pore breakthrough with “Primer C” would additionally limit the binder migration, because binder migration from one place to the other relies on an interconnected liquid phase between the two places. If the upper part is partially dry before capillary transport reaches the primer, these regions cannot take up additional binder coming from the bottom of the electrode. A measurement technique that allows a statement about the vertical distribution of the saturation is cryoSEM.<sup>[24]</sup> **Figure 5** shows vertical cross-sections of drying multilayers “SBR100 on Primer C”. The drying is stopped at  $\approx 120$  s (left) and  $\approx 200$  s (right), before and after a pore breakthrough has been observed ( $\approx 160$  s) via the microscope beneath the sample.

In **Figure 5**, empty pores are observable by blue, indicating chlorine from a NaCl-supporting substrate below the copper. The NaCl support is relevant for sample preparation. The chlorine deposits in already empty pores during the broad ion beam milling. **Figure 5**, left gives the impression that the pore system has started to empty. Empty regions marked by chlorine appear over the top half of the film. There is still a fully saturated region shown by the strong signal for water (green) between the graphite and the substrate. The primer is still a fully closed layer. No pore breakthrough through the primer is visible at the bottom of the electrode. In the sample after the pore breakthrough (**Figure 5**, right), almost the entire cross-section is emptied except minor areas near the substrate. Parts of the solvent in these regions may have been transported by capillary transport from out of the primer layer. The remaining solvent directly in contact with the substrate suggests that a proportion of the primer layer remains in place. This impression is given by the microscope image (View from below at 200 s) as well. Even if there is no fully closed primer layer, enough of the material remains in clusters to support adhesion. Vice versa, the fact that there is no closed primer layer suggests that not only solvent but some of the material (binder, CB, LAPONITE) as well have been transported by capillarity throughout the porous system of the electrode coating. This explanation fits well to the drop in adhesion strength due to binder migration.

#### 2.4. Transfer of Concept toward Material-Efficient Battery Electrodes

The goal of an optimization via a simultaneously coated primer layer is to reach the best possible connection between substrate and electrode coating, while using as little binder content as possible in the complete electrode (primer and electrode coating). We chose “Primer C” as most promising basis for an optimization of the electrode. **Figure 6** shows the possible savings by the multilayer approach.

The estimation reveals that there is about one-third more water to be dried with the primer. However, savings in SBR areal mass loading are significant with 70% less SBR for “SBR0 on Primer C” than for a “Single Layer SBR100”. If these SBR-reduced electrodes can be dried faster this would increase the throughput of an industrial dryer (limited by dryer length), despite additional solvent. Thus, the influence of these changes is investigated, again, for increasing drying rate by adhesion, electrical interface resistance, and C-Rate capability characterization. **Figure 7** shows the adhesion strength and interface resistance for the simultaneously coated multilayers with fixed primer formulation “Primer C” and varying electrode formulation “SBR100” with 100% of the initial SBR, “SBR50” and “SBR0” with no SBR in the anode slurry.

The trend for a falling adhesion strength with decreasing the SBR-binder content for “Single Layer SBR100” electrodes<sup>[17]</sup> is met also for the SBR-reduced simultaneously coated multilayer electrodes “SBR50 on Primer C” and “SBR0 on Primer C”. All samples show binder migration by a decrease of adhesion strength for increasing drying rate.

Even for “SBR0 on Primer C”, the adhesion strength is higher than for the “Single Layer SBR100” electrodes for all drying rates investigated. This suggests that even for higher drying rates, a considerable amount of SBR is preserved near the substrate. For low drying rates, interlayer delamination between primer and electrode occurred for “SBR0 on Primer C” (S1, Supporting Information). If enough primer remained at the substrate to form a closed layer and little enough SBR was present in the

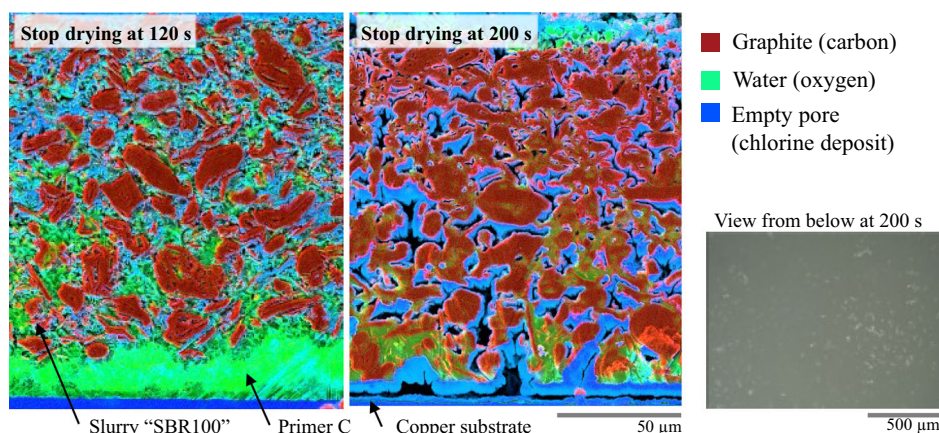


**Figure 5.** CryoSEM-energy-dispersive X-ray spectroscopy (EDS) cross section for two separate electrodes “SBR100 on Primer C” ( $0.75 \text{ g m}^{-2} \text{ s}^{-1}$ ) quenched before (120 s) and after a pore breakthrough (200 s) has been observed ( $\approx 160$  s) via the microscope beneath the sample (view from below). Additional microscope pictures can be found in S3, Supporting Information. Empty pores are observable by blue, indicating chlorine and copper from a NaCl support below the copper substrate. The chlorine deposits in already empty pores during the broad ion beam milling.

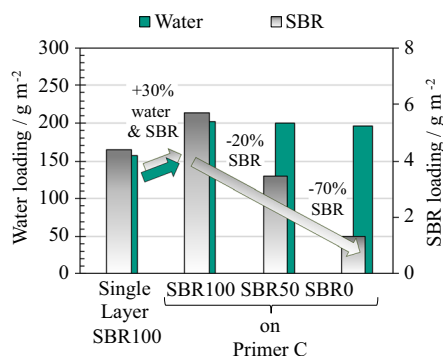


**Figure 6.** Estimation of SBR content in the multilayer electrodes for a  $4.2 \text{ mAh cm}^{-2}$  electrode ( $110 \text{ g m}^{-2}$  graphite) with “Primer C” ( $2.6 \text{ g m}^{-2}$ , dry). There is about one-third more water to be dried. Savings in SBR areal mass loading are significant. Up to 70% less SBR for “SBR0 on Primer C” than for “Single Layer SBR100”.

electrode coating, the delamination must occur at the weakest interface (between primer and electrode coating). For increasing drying rates, we observed a transition from an interlayer delamination to a full delamination. The most obvious explanation for this behavior is that more primer is displaced by binder migration for increasing drying rate.

Parallel to decreasing adhesion strength, binder migration leads, as well for the multilayers made with “SBR50” and “SBR0”, to an increased interface resistance. However, the samples differ in the level of interface resistance: the higher the adhesion strength the lower the interface resistance. It is noteworthy that, even if interface resistance follows this trend, the composite volume resistivity follows the inverse trend falling by 40% from “SBR100” to “SBR0” (S6, Supporting Information).

In the end of the process chain, the most important optimization criterion is the C-rate capability and long-term stability of the electrodes in operation. Calendered samples were tested as full cell coin cells for increasing C-rate. **Figure 8** shows the 2C-discharge capacity (cathode) of the simultaneously coated multilayer electrodes “SBR100 on Primer C”, “SBR50 on

Primer C”, “SBR0 on Primer C” as well as “Single Layer SBR100” electrodes for a LDR of 0.75 and HDR of  $6 \text{ g m}^{-2} \text{ s}^{-1}$ . The full C-rate tests for each drying rate can be found in S4 and S5, Supporting Information. The initial discharge capacity of the cathodes (C/20) paired with the samples containing “Primer C” is not influenced by the primer. Limiting for higher C rate (3C) are the cathodes made with Nickel manganese cobalt oxide (NCM)622.

Figure 8 shows that for a C-rate of 2C (discharge in half an hour), no significantly worse discharge capacity of “SBR100 on Primer C” can be found for the low drying rate of  $0.75 \text{ g m}^{-2} \text{ s}^{-1}$  compared to “Single Layer SBR100”. This suggests a remain of most of the (binder) material comprised in “Primer C” near the current collector and a closed, intact primer layer (see SEM, Figure 3). However, for increasing the drying rate and thus displacement of the additional binder comprised in “Primer C”, the discharge capacity drops by 20% compared to “Single Layer SBR100”. The accumulation even could be visualized (see SEM Figure 3).

Working around this binder accumulation, a gradual reduction of SBR content from “SBR100 on Primer C” over “SBR50 on Primer C” to “SBR0 on Primer C” leads to significant improvements in the C-Rate capability. For the higher drying rate, the sample “SBR0 on Primer C” shows the highest remaining 2C-discharge capacity of  $103.3 \pm 1.9 \text{ mAh g}^{-1}$ . It is noteworthy that this even exceeds the discharge capacity of  $94.0 \pm 2.2 \text{ mAh g}^{-1}$  for “Single Layer SBR100” dried at 8-times lower drying rate, that is, while maintaining an adhesion strength several times higher than “Single Layer SBR100” (see Figure 2, left). With up to 70% less SBR-binder in the system, there is a trend toward generally less impact of the drying rate on the C-rate capability, as less binder is available to be displaced by capillary transport.

The positive effect of the simultaneously coated primer layer on the adhesion strength and interface resistance does also show an impact in a longer-term cycling of the electrode. In a symmetric 1C/1C charge-discharge test, the deterioration of specific discharge capacity is expected to resemble the transport resistances in the cell. The focus lies on the higher drying rate (more binder migration). **Figure 9 a)** shows the 1C-discharge capacity of NCM622 cathodes matched with the electrodes “SBR100 on

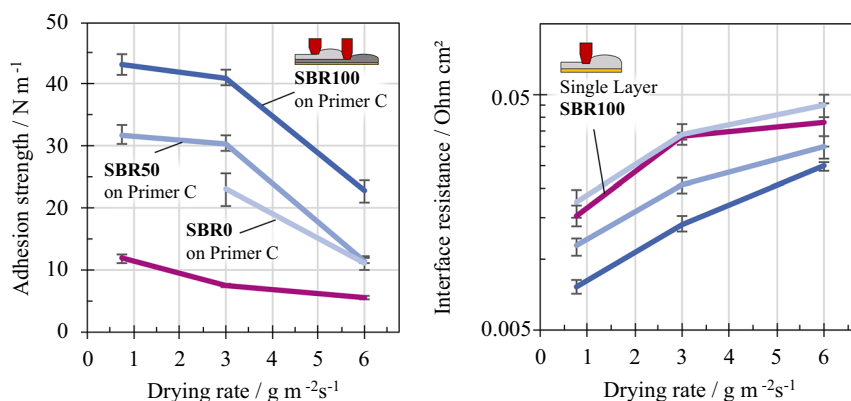


**Figure 7.** Adhesion strength and electrical interface resistance versus drying rate for simultaneously coated multilayers “SBR100 on Primer C”, “SBR50 on Primer C”, and “SBR0 on Primer C” with “Primer C” as bottom layer among “Single Layer SBR100” electrodes. Even with half or no SBR left in the electrode coating, the adhesion strength is significantly increased by the primer. Interface resistance increases by binder migration, but is kept on a level even or lower than the “Single Layer SBR100” electrodes.



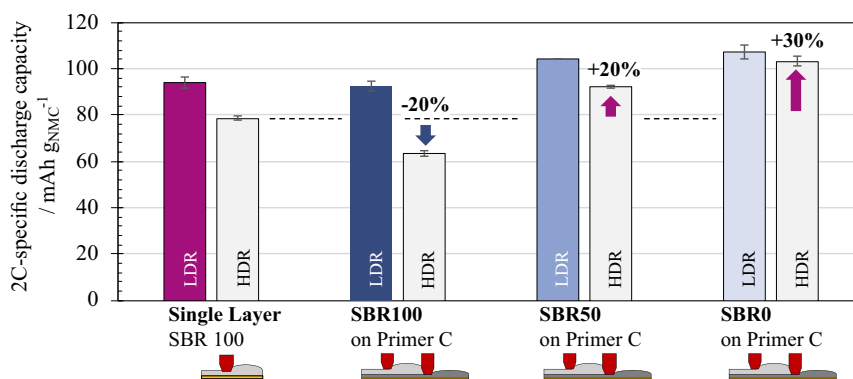


**Figure 8.** 2C-specific discharge capacity (NCM622 cathode) matched with the simultaneously coated multilayer electrodes “SBR100 on Primer C”, “SBR50 on Primer C”, “SBR0 on Primer C” as well as the “Single Layer SBR100” electrodes for a LDR of  $0.75 \text{ g m}^{-2} \text{ s}^{-1}$  and HDR  $6 \text{ g m}^{-2} \text{ s}^{-1}$ . Additional binder leads to worse C-rate capability.<sup>[17]</sup> Less binder in the system, due to its use only in the primer layer, benefits the C-rate capability especially for increasing drying rate. Average of at least two cells is shown. The full C-rate tests for each drying rate can be found in Section S4 and S5, Supporting Information.

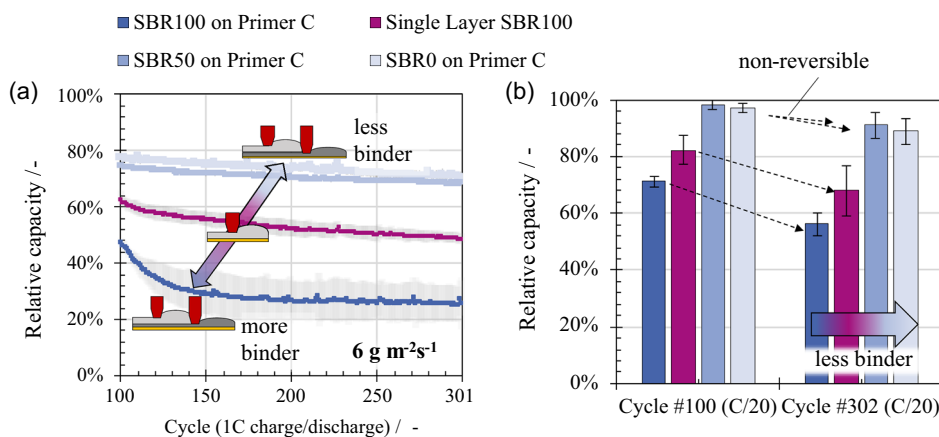


**Figure 9.** a) Relative capacity (1C-discharge capacity/C/20-discharge capacity of formation cycle) of NCM 622 cathodes matched with the electrodes “SBR100 on Primer C”, “SBR50 on Primer C”, and “SBR0 on Primer C” as well as “Single Layer SBR100” for the higher drying rate of  $6 \text{ g m}^{-2} \text{ s}^{-1}$ . Cycling with the same cells directly after the foregoing C-rate capability test. Charging is with 1C to show transport resistances in the cell. Additional binder leads to increased ionic resistance and a faster deterioration,<sup>[17]</sup> if migration occurs. Size of deviations follows the deterioration. b) Relative capacity of the recovery cycles (C/20 cycles #100 & #302). Comparison of cycle #100 with #302 shows the irreversible deterioration. Average of at least two cells is shown.

Primer C”, “SBR50 on Primer C”, and “SBR0 on Primer C” as well as “Single Layer SBR100” for the higher drying rate of  $6 \text{ g m}^{-2} \text{ s}^{-1}$ . The cycles are after the foregoing test on C-Rate capability (cycling protocol, Table 5). Cycles #100 as well as #302 were done at C/20 to show how much of the deterioration of capacity is reversible (just transport resistances) or nonreversible (permanent losses) in Figure 9 b).

The deterioration of capacity over longer cycling with symmetric 1C/1C charge/discharge is strong for the samples dried at higher drying rate as ionic resistances are high. Reduction of binder content and combination with the primer partially negate this as there is a lower ionic resistance (with less SBR present) expected. With a faster deterioration of “SBR100 on Primer C” than “Single Layer SBR100”, the order of capacity retention resembles the overall SBR content of the electrodes. A C/20 step before (cycle #100) and after the long-term 1C/1C charge/discharge test (cycle #302) shows the deterioration of specific

capacity that is nonreversible after one recovery cycle. Here, again, the SBR-reduced simultaneously coated multilayers “SBR50 on Primer C” and “SBR0 on Primer C” outperform the “Single Layer SBR100” and the simultaneously coated multilayer with additional binder “SBR100 on Primer C”. There is no direct correlation between adhesions strength and non-reversible deterioration. In the recovery cycles, they reach over 90% of their initial capacity (compared to cycle #2), respectively.

### 3. Conclusion

In this work, we investigated the use of simultaneously coated primer layers for structural optimization of electrodes. The multilayer system was optimized under the criterion that drying at high drying rates should have minimal negative effect on



adhesion strength, interface resistance, and C-rate capability. The SBR-content of the electrodes was aimed to be minimized.

It can be shown that binder migration is also happening for fast drying of simultaneously coated multilayers of primer and electrode. Depending on the formulation of the primer, its ability to partially remain between electrode coating and current collector is crucial for promoting adhesion strength and interface resistance. A primer with LAPONITE, forming an interconnected network, and thus resistance against being displaced, was found to be suitable to make a simultaneously coated primer layer beneficial for adhesion strength and interface resistance. The primer partially remains during drying, even for higher drying rate.

With fixed primer formulation, the formulation of the electrode coating was adapted toward a minimization of SBR-binder concentrations (less SBR beneficial for ionic resistance). The function of the primer coating to improve the adhesion, especially for electrode coatings that show a lack of adhesion was found to be met by an over 200% higher adhesion strength. Like this, the SBR content could be decreased by 100% in the electrode coating leading to electrodes that are processable at 8 times higher drying rate. In addition to 70% savings of SBR material (little amount still in the primer), an over 30% improved specific discharge capacity at 2C could be reached compared to the single layer reference. The use of additional water in the primer pays out by the possibility to increase the drying rate, which means a reduction of the drying time from over 200 s to  $\approx 30$  s.

This successful and promising test series for graphite anodes is to be transferred to other material systems that lack of sufficient adhesion and electrical interface connection, like porous, nanostructured particles,<sup>[25]</sup> and materials for sodium-ion batteries like sodium (Na) vanadium phosphate (NVP) and Prussian Blue Analogues (PBA).

## 4. Experimental Section

**Materials and Mixing:** The CMC-solutions (Sunrose MAC500LC, Nippon Paper Industries, Japan) were made with a laboratory stirrer with 42 mm dissolver stirrer (IKA, Germany). For the LAPONITE dispersions, first LAPONITE-RD (BYK-Chemie GmbH, Germany) was dispersed in water for about 10 min until a bluish transparent dispersion was obtained. CMC was added under stirring and dissolved within 30-45 min until a transparent solution was obtained.

The slurries and primers were mixed in a dissolver (Dispermat SN-10, VMA Getzmann GmbH Verfahrenstechnik, Germany). The container was cooled during the process. First, CB (Super C65, Timcal SA, Switzerland) was dispersed in a 2 wt-% CMC (Sunrose MAC500LC, Nippon Paper Industries, Japan) solution at 1500 rpm for 30 min containing the LAPONITE already, if present in the respective formulation. For the slurries, the graphite (SMGA, Hitachi Chemical Co. Ltd., Japan) was added in three steps with short mixing steps of about a minute at 400 rpm. Further water was added for the final solid content. A second dispersion step followed (30 min, 1500 rpm). In the final step, SBR (Zeon Europe GmbH, Japan) was added as dispersion in water and the slurry/primer was mixed for 10 min at 500 rpm and degassed. The composition was chosen so that the dry electrode has the composition in Table 1. The viscosity was measured by a rotational viscometer Physica MCR 101 (Anton Paar, Germany) with a plate-plate geometry (25 mm diameter) from 0.01 to 1.000 s<sup>-1</sup> at 25 °C.

**Electrode Coating and Drying:** The coating and drying of the graphite slurries were carried out in a discontinuous process as described by Baunach et al.<sup>[26]</sup> The 10  $\mu$ m copper current collector (Civen Metal Material Co. Ltd., China) was attached to a temperature-controlled plate via

vacuum. The coating of the anode slurries was applied with a doctor blade ZUA 2000.60 (Zehntner GmbH, Switzerland) and subsequently, the coating was run under the drying nozzles of an impingement dryer.

For simultaneous multilayer coating, two doctor blades ZUA 2000.60 were joined.

For homogeneous drying, the plate was periodically moved under the dryer until the slurry was dry. The drying temperature and heat transfer coefficient were set independently to separate their respective effects. For all experiments, the drying rate was set by adjusting the temperature of the heated plate and maintaining a constant heat transfer coefficient of the slot nozzle dryer, considering the dew point of the drying air. **Table 4** shows the drying rates, the heat transfer coefficients, and the drying temperatures.

**Electrode Characterization:** The porosity was calculated from the areal mass loading divided by the layer thickness and the density of the dry mixture of the components. The electrodes (Figure 3) were imaged with a field-emission scanning electron microscope (Supra 55, Carl Zeiss GmbH, Germany) equipped with an EDS detector (Ultim Extreme, Oxford Instruments, UK). The cross-sectional samples of the slightly calendered electrodes were prepared through ion-beam milling (EM TIC3X, Leica Microsystems GmbH, Germany) using argon ions at an accelerating voltage of 6 kV and a gun current of 2.2 mA.

The cryoSEM images (Figure 5) were taken from electrode samples frozen in a nitrogen slush. The preparation of a cross-section of the slurry was done under liquid nitrogen using a diamond saw with a NaCl support plate. The samples were transferred via a nitrogen-cooled shuttle (Leica VCT100, Leica Camera AG, Germany) into a cryogenic broad-ion-beam treatment (Leica TIC3X, Leica Camera AG, Germany). Ion sputtering was conducted producing a smooth surface (3–4 h, 8.5 kV). The observation of the samples in a cryo-SEM (Zeiss Supra 55, equipped with an Oxford Instruments X-Max150 EDS detector) was conducted at 3 kV acceleration voltage for high-resolution micrographs and at 12 kV acceleration for electron images in combination with EDS, respectively, at a pressure of 2 E-005 mbar and a temperature of  $-130$  °C.

**Adhesion Strength and Resistivity Measurements:** To determine the adhesion strength between the current collector and the dried electrodes, a 90° peel test was carried out with a universal testing machine AMETEK LS1 (Lloyd Instruments Ltd., UK) and a 10 N load cell. All samples of the dried anodes were cut out with a width of 30 mm and attached with the coated side to an adhesive strip. The sample was pressed on by rolling once with a cylindrical weight of 10 kg to ensure uniform contact between the coating and the adhesive strip. The current collector foil was then peeled off the coating at a constant speed of 600 mm min<sup>-1</sup> at a 90° angle using the testing machine. The resulting pull-off force was measured and divided by the sample width to obtain a line force.

The resistivity was determined with an electrode resistance measurement system (RM2610, Hioki, Japan) using uncalendered samples.

**Full Cell Coin Cell Tests:** The anodes were electrochemically examined in coin full cells (CR 2032, Hohsen Corp., Japan) against a NMC622 (BASF SE, Germany) counter electrode with a loading of 3.85 mAh cm<sup>-2</sup> (10% balancing).

The anodes were calendered to match a porosity of  $44.9 \pm 0.5\%$  with a total deviation of thickness of 6  $\mu$ m. Before the assembly of the cells, the electrodes were postdried in a vacuum oven (110 °C, 16 h) to evaporate

**Table 4.** Overview of the drying rates and the drying temperatures with a constant heat transfer coefficient of 35 W m<sup>-2</sup> K<sup>-1</sup>. The dew point for the experiments ranged from  $-1$  to 14 °C. The drying temperature was set according to the dew point on the experiments' day.

Drying rate [g m <sup>-2</sup> s <sup>-1</sup> ]	Heat transfer coefficient [W m <sup>-2</sup> K <sup>-1</sup> ]	Film temperature range [°C]
0.75	35	27.6–31.7
3	35	49.9–51.4
6	35	62.7–63.4

**Table 5.** Cycling protocol for full cell coin cell tests. C-rate capability with symmetric long-term cycling at 1C for 300 cycles (stress test).

Cycle	C rate charge	C rate discharge
1–2	0.05	0.05
3–12	0.5	0.5
13–52	1	1, 2, 3, 4, 5 (10 cycles)
53–98	1	1
99–100	1	0.05
101–300	1	1
301	1	0.05
302	0.05	0.05

any residual water. The electrolyte used was LP30 (Merck KGaA, Germany) with the conductive salt 1M LiPF<sub>6</sub> in an ethylene carbonate (EC), dimethyl carbonate (DMC) mixture (EC/DMC = 50/50, v/v). As separator, a glass-microfiber fleece (GF/C, Whatman plc, UK) was used. The cells were assembled in an argon-filled glovebox and sealed with an MSK-11 press (MTI Corp., USA). Cycling was carried out in a constant current mode inside a voltage range of 3–4.3 V. The cycling protocol can be found in **Table 5**.

## Supporting Information

Supporting Information is available from the Wiley Online Library or from the author.

## Acknowledgements

This work contributes to the research performed at CELEST (Center for Electrochemical Energy Storage Ulm Karlsruhe) and Material Research Center for Energy Systems (MZE). It was funded by the Deutsche Forschungsgemeinschaft (DFG, German Research Foundation) under Germany's Excellence Strategy – EXC 2154 – Project number 390874152 (POLiS Cluster of Excellence). The authors would like to thank for support of others involved in this work (Max Buck, electrode coating and characterization and Dr. Joyce Schmatz, cryoSEM measurements).

Open Access funding enabled and organized by Projekt DEAL.

## Conflict of Interest

The authors declare no conflict of interest.

## Data Availability Statement

The authors declare that the data supporting the findings of this study are available within the paper and the Supplementary Information file. Additional data and metadata, will be made available in a Zenodo repository with DOI <https://doi.org/10.5281/zenodo.13880280>.

## Keywords

adhesion strength, binder migration, electrode processing, lithium-ion batteries, microstructure optimization

Received: August 29, 2024

Revised: October 7, 2024

Published online:

- [1] J. Fleischmann, M. Hanicke, E. Horetsky, D. Ibrahim, S. M. Linder, P. Schaufuss, L. Torscht, A. van de Rijt, **2023**.
- [2] R. Diehm, M. Müller, D. Burger, J. Kumberg, S. Spiegel, W. Bauer, P. Scharfer, W. Schabel, *Energy Technol.* **2020**, *8*, 2000259.
- [3] K. Park, H. E. Yoo, Y. Jung, M. Ryu, S. Myeong, D. Lee, S. C. Kim, C. Kim, J. Kim, J. Kwon, K. Lee, C.-W. Cho, U. Paik, T. Song, *J. Power Sources* **2023**, *577*, 233238.
- [4] Y. Arai, N. Kobayashi, S. Doi, H. Yokouchi, M. Ohmori, Method for producing collector for electrochemical elements, method for producing electrode for electrochemical elements, collector for electrochemical elements, electrochemical element, and coating liquid for forming collector for electrochemical elements, EP2838145B1, **2013**.
- [5] H. Yokouchi, M. Omori, A. Takeda, 塗工液、集電体および集電体の製造方法. **2012**.
- [6] A. Takeda, T. Nakamura, H. Yokouchi, Current collector for electrical storage device, method for manufacturing same, and coating liquid used for manufacturing same, EP3651248A1, **2018**.
- [7] S. Spiegel, A. Hoffmann, J. Klemens, P. Scharfer, W. Schabel, *J. Coat. Technol. Res.* **2024**, *21*, 493.
- [8] S. K. Lee, T. Haze, S. J. Cho, Primer-coated copper foil having superior adhesive strength and method for producing the same, US20140186581A1, **2013**.
- [9] J. Klemens, D. Burger, L. Schneider, S. Spiegel, M. Müller, N. Bohn, W. Bauer, H. Ehrenberg, P. Scharfer, W. Schabel, *Energy Technol.* **2023**, 2300267, <https://doi.org/10.1002/ente.202300267>.
- [10] J. Kumberg, About Drying of Hierarchically Structured Electrodes for High Energy Li-Ion Battery Applications. Karlsruher Institut für Technologie, Karlsruhe **2022**.
- [11] R. Diehm, J. Kumberg, C. Dörrer, M. Müller, W. Bauer, P. Scharfer, W. Schabel, *Energy Technol.* **2020**, *8*, 1901251.
- [12] J. Kumberg, W. Bauer, J. Schmatz, R. Diehm, M. Tönsmann, M. Müller, K. Ly, P. Scharfer, W. Schabel, *Energy Technol.* **2021**, <https://doi.org/10.1002/ente.202100367>.
- [13] D. Liu, L. Chen, T. Liu, W. Chu, C. Tiu, *Energy Technol.* **2017**, *5*, 1235.
- [14] L.-C. Chen, D. Liu, T.-J. Liu, C. Tiu, C.-R. Yang, W.-B. Chu, C.-C. Wan, *J. Energy Storage* **2016**, *5*, 156.
- [15] D. Burger, J. Klemens, N. Keim, M. Müller, W. Bauer, J. Schmatz, J. Kumberg, P. Scharfer, W. Schabel, *Energy Technol.* **2022**, *12*, 2400057.
- [16] A. Heinzl, B. Capraro, B. Oberschachtsiek, Entwicklung industrieller Beschichtungsverfahren für Li-Ionen-Batterien auf Basis umweltfreundlicher Bindersysteme. Innov. IGF Forschungsvorhabensnummer 18437 BG **2017**.
- [17] K. Hofmann, A. D. Hegde, X. Liu-Theato, R. Gordon, A. Smith, N. Willenbacher, *J. Power Sources* **2024**, *593*, 233996.
- [18] J. A. E. W. O. O. K. Nam, M. A. R. C. I. O. S. Carvalho, *J. Fluid Mech.* **2009**, *631*, 397.
- [19] J. Kumberg, M. Müller, R. Diehm, S. Spiegel, C. Wachsmann, W. Bauer, P. Scharfer, W. Schabel, *Energy Technol.* **2019**, *7*, 1900722.
- [20] B. Westphal, H. Bockholt, T. Günther, W. Haselrieder, A. Kwade, *ECS Trans.* **2015**, *64*, 57.
- [21] M. Baunach, S. Jaiser, S. Schmelzle, H. Nirschl, P. Scharfer, W. Schabel, *Dry. Technol.* **2016**, *34*, 462.
- [22] S. Jaiser, N. Sanchez Salach, M. Baunach, P. Scharfer, W. Schabel, *Dry. Technol.* **2017**, *35*, 1807.
- [23] J. Kumberg, M. Baunach, J. C. Eser, A. Altvater, P. Scharfer, W. Schabel, *Energy Technol.* **2021**, *9*, 2100013.
- [24] S. Jaiser, J. Kumberg, J. Klaver, J. L. Urai, W. Schabel, J. Schmatz, P. Scharfer, *J. Power Sources* **2017**, *345*, 97.
- [25] J. Klemens, L. Schneider, E. C. Herbst, N. Bohn, M. Müller, W. Bauer, P. Scharfer, W. Schabel, *Energy Technol.* **2022**, *10*, 2100985.
- [26] M. Baunach, S. Jaiser, P. Cavadini, P. Scharfer, W. Schabel, *J. Coat. Technol. Res.* **2015**, *12*, 915.